Structure and Mutational Analysis of the PhoN Protein of Salmonella typhimurium Provide Insight into Mechanistic Details ‡

ARTICLE *in* BIOCHEMISTRY · MARCH 2007

Impact Factor: 3.02 · DOI: 10.1021/bi062180g · Source: PubMed

3 AUTHORS, INCLUDING:

Ravindra D Makde
Bhabha Atomic Research Centre
19 PUBLICATIONS **333** CITATIONS
SEE PROFILE

Vinay Kumar
Bhabha Atomic Research Centre
33 PUBLICATIONS **538** CITATIONS
SEE PROFILE

Structure and Mutational Analysis of the PhoN Protein of *Salmonella typhimurium* Provide Insight into Mechanistic Details‡

Ravindra D. Makde,§ Suresh K. Mahajan,|| and Vinay Kumar*,§

High Pressure Physics Division, Bhabha Atomic Research Centre, Mumbai 400 085, India, and The Institute of Science, Madam Cama Road, Mumbai 400 032, India

Received October 20, 2006; Revised Manuscript Received December 14, 2006

ABSTRACT: The *Salmonella typhimurium* PhoN protein is a nonspecific acid phosphatase and belongs to the phosphatidic acid phosphatase type 2 (PAP2) superfamily. We report here the crystal structures of phosphate-bound PhoN, the PhoN−tungstate complex, and the T159D mutant of PhoN along with functional characterization of three mutants: L39T, T159D, and D201N. Invariant active site residues, Lys-123, Arg-130, Ser-156, Gly-157, His-158, and Arg-191, interact with phosphate and tungstate oxyanions. Ser-156 also accepts a hydrogen bond from Thr-159. The T159D mutation, surprisingly, severely diminishes phosphatase activity, apparently by disturbing the active site scaffold: Arg-191 is swung out of the active site resulting in conformational changes in His-158 and His-197 residues. Our results reveal a hitherto unknown functional role of Arg-191, namely, restricting the active conformation of catalytic His-158 and His-197 residues. Consistent with the conserved nature of Asp-201 in the PAP2 superfamily, the D201N mutation completely abolished phosphatase activity. On the basis of this observation and in silico analysis we suggest that the crucial mechanistic role of Asp-201 is to stabilize the positive charge on the phosphohistidine intermediate generated by the transfer of phosphoryl to the nucleophile, His-197, located within hydrogen bond distance to the invariant Asp-201. This is in contrast to earlier suggestions that Asp-201 stabilizes His-197 and the His^{197}−Asp^{201} dyad facilitates formation of the phosphoenzyme intermediate through a charge-relay system. Finally, the L39T mutation in the conserved polyproline motif (^{39}LPPPP^{43}) of dimeric PhoN leads to a marginal reduction in activity, in contrast to the nearly 50-fold reduction observed for monomeric *Prevotella intermedia* acid phosphatase, suggesting that the varying quaternary structure of PhoN orthologues may have functional significance.

Bacterial nonspecific acid phosphohydrolases (bNSAPs, EC 3.1.3.2) are secreted enzymes, functioning as soluble periplasmic proteins or as membrane-bound lipoproteins (*1*). They are a diverse group of monomeric or oligomeric proteins and exhibit optimal catalytic activity at acidic to neutral pH. The monomer molecular mass is in the range of 25−30 kDa. On the basis of amino acid sequence analysis, bNSAPs have been classified into three distinct molecular families, designated as class A, B, and C, respectively (*2*). These enzymes can dephosphorylate disparate phosphate monoesters in the periplasmic space, thus enabling organic moieties to enter the cell.

The *phoN* genes of *Salmonella enterica* serover *typhi* (*S. typhi*) and *Salmonella enterica* serover *typhimurium* (*S. typhimurium*) encode 250 amino acid polypeptides, 20 of which function as signal peptides for periplasmic localization (Swiss-Prot accession numbers Q934J6 and P26976). The 26 kDa periplasmic PhoN protein is a member of the class A bNSAPs and belongs to the PAP2[1] superfamily [Pfam accession number PF01569 (*3*)]. Other members of the PAP2 superfamily include vanadium-dependent chloroperoxidases, glucose-6-phosphatase, and lipid phosphate phosphatases. The PAP2 superfamily members share a conserved sequence motif, which consists of three noncontiguous polypeptide fragments: motif 1, KX_6RP; motif 2, PSGH; and motif 3, SRX_5HX_3D.

Crystal structures of vanadium-dependent chloroperoxidases and class A bNSAPs of *Escherichia blattae* are available in the Protein Data Bank (PDB codes 1VNC and 1D2T, respectively). The active site scaffold of class A bNSAPs consists of Lys-123, Arg-130, Ser-156, Gly-157, His-158, Arg-191, and His-197 (numbering as per the PhoN sequence). While Lys-123, Arg-130, Ser-156, Gly-157, His-158, and Arg-191 residues are thought to interact with the phosphate of organophosphate substrate (Figure 1A), cleavage of the O−P bond is expected to be carried out by two histidyl residues: His-158 and His-197. It is generally accepted that His-197 carries a nucleophilic attack at the electron-deficient phosphorus center, leading to the formation

‡ The atomic coordinates and structure factors for the native PhoN, PhoN−tungstate complex, and T159D mutant of PhoN have been deposited in the Protein Data Bank under the accession codes 2A96, 2AKC, and 2IPB, respectively.

* To whom correspondence should be addressed. Tel: +91-22-25593761. Fax: +91-22-25505151. E-mail: vinay@barc.gov.in.

§ Bhabha Atomic Research Centre.

|| The Institute of Science.

[1] Abbreviations: *p*NPP, *p*-nitrophenyl phosphate; IPTG, isopropyl *β*-D-thiogalactopyranoside; SDS, sodium dodecyl sulfate; PhoN, PhoN protein of *Salmonella typhimurium*; Pho, PhoN orthologue from *Escherichia blattae*; PAP2, phosphatidic acid phosphatase type 2; rms, root mean square.

10.1021/bi062180g CCC: $37.00
Published on Web 01/31/2007

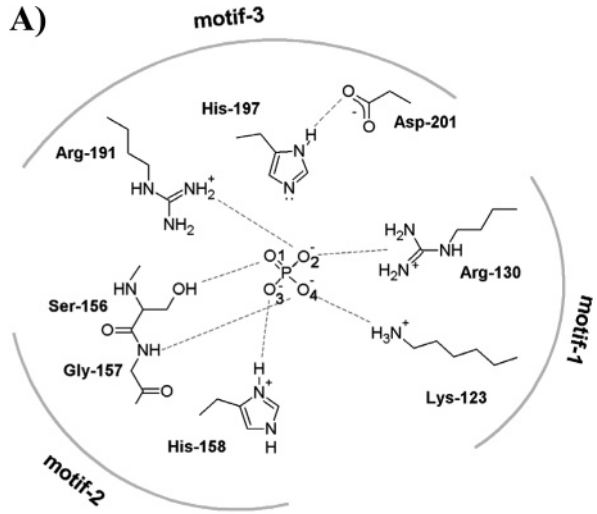

B)

	motif-1			motif-2				motif-3			
	K-X_6----R-----P(X_{12-54})P-------S------G-----H(X_{31-54})S---RX_5----HX_3-----D										
	K	R	P	P	S	G	H	S	R	H	D
NSAP-PI		●					●		●	●	
NSAP-EC					●				●		
G6P	●	●					●		●	●	
LPP1	●	●	●		●	○	●		●	●	
DGPP		●					◐			●	
VCPO	◐	◐					●		●	●	

FIGURE 1: (A) Schematic of active site residues and their interactions with the substrate phosphate of *S. typhimurium* PhoN. The figure was prepared using ACD/ChemSketch version 10. (B) Effect of mutagenesis of the residues of the conserved motif on the phosphatase activity of PAP-2 proteins. The black filled circle indicates less than 5% retention of enzymatic activity; the gray filled circle indicates 5−20% retention of enzymatic activity; the open circle indicates nearly 40% retention of enzymatic activity. The blank box indicates that mutational data are not available. Key: NSAP-PI, nonspecific acid phosphatase of *P. intermedia* (*9*); NSAP-EC, nonspecific acid phosphatase of enteroinvasive *E. coli* (*10*); G6P, glucose 6-phosphatase of human (*11*); LPP1, lipid phosphate phosphatase 1 of rat (*12*); DGPP, diacylglycerol pyrophosphate phosphatase of *S. cerevisiae* (*13*); VCPO, vanadium-dependent chloroperoxidase of *C. inaequalis* (*14*).

of a phosphohistidine intermediate, and His-158 acting as a general acid/base facilitates the release of the alcohol and inorganic phosphate during the catalytic cycle (*4*, *5*). A similar reaction mechanism is expected to be operating in other PAP2 proteins (*4*, *6*), as the active site residues of bacterial acid phosphatases are part of the conserved PAP2 sequence motif [KX_6RP-(X_{12-54})-PSGH-(X_{31-54})-SRX_5-HX_3D] (*4*, *5*, *7*, *8*). The functional importance of several of these residues has been verified by mutational analysis, which is summarized in Figure 1B.

The inorganic phosphate released in the periplasmic space can promote precipitation of heavy metal ions, and this property can be exploited for bioremediation of heavy metal wastes (*15*). Basnakova et al. (*16*) advocated the engineering of PhoN, as *Escherichia coli* harboring the *phoN* gene of *S. typhi* on a multicopy plasmid has been found to most efficiently remove uranyl and nickel ions from diluted solutions. Structure−function-based "rational" engineering for altering the pH optimum of the PhoN protein has recently been attempted (*17*). A detailed dissection of the functional role of the activity-linked residues will help to elucidate mechanistic details of the phosphatase reaction and the determinants of the pH−activity profile that can be targeted for engineering PhoN for the desired characteristics.

Here, we report the use of site-directed mutagenesis in conjunction with biochemical characterization and crystal structure analysis to elucidate the role of the activity-linked residues. We show that His-158 and His-197 are in $N^{\epsilon 2}$-H and $N^{\delta 1}$-H tautomeric forms, respectively, that tungstate mimics the phosphoenzyme intermediate, that a T159D substitution produces near total loss of the phosphatase activity, and that the D201N mutant does not possess phosphatase activity over a broad pH range. A critical functional role for Arg-191 based on steric restriction of the side-chain imidazole groups of catalytic histidine residues is demonstrated for the first time. Asp-201 makes a crucial contribution to the phosphatase activity, most likely by stabilizing the positively charged phosphoenzyme intermediate. Further, the substitution of distal Leu-39 with Thr produced only a marginal decrease in the enzymatic efficiency of *Salmonella typhimurium* PhoN, indicating that the varying oligomeric states of PhoN orthologues from different bacteria could have functional significance.

EXPERIMENTAL PROCEDURES

Materials. dNTPs and T4 DNA ligase were obtained from Roche and restriction enzymes from New England BioLabs. *E. coli* XL1 Blue [*recA1 endA1 gyrA96 thi-1 hsdR17* (r_k^-, m_k^+) *supE44 relA1* lac (F′ proAB $lacI^qZ\Delta M15$ Tn10-tet^r)], the QuickChange site-directed mutagenesis kit, and *pfu-turbo* DNA polymerase were obtained from Stratagene. *E. coli* BL21(DE3) [*E. coli* B F^- *dcm ompT hsdS* (r_B^- m_B^-) *galλ*-(DE3)] and pET21a(+) plasmid were from Novagen. Oligonucleotides for cloning and mutagenesis were synthesized at BRIT. *p*-Nitrophenyl phosphate and other fine chemicals were procured from SRL.

Site-Directed Mutagenesis of phoN, Overexpression, and Purification of Mutants. All basic recombinant DNA procedures were performed as described by Sambrook and Russell (*18*). *E. coli* XL1 Blue and BL21(DE3) were used for transformation of the plasmids and expression of the genes, respectively. The pET21a-*phoN* wild-type construct (*17*) was used as a template to carry out the site-directed mutagenesis of *phoN* employing the QuickChange site-directed mutagenesis kit. The complementary primer pairs used for *phoN* mutagenesis were as follows: D201N (left, CACTGGCAAAGC**AAT**GTTGATGCTGGCCG; right, CGGCCAGCATCAACATTGCTTTGCCAGTG), T159D (left, CCCTTCCGGGCAT**GAT**GCTTATAGTACAC; right, GTGTACTATAAGCATCATGCCCGGAAGGG), and L39T (left, GTCAGTTCTAC**ACA**CCACCACCGCCAG; right CTGGCGGTGGTGGTGTGTAGAACTGAC), where the bold letters in the left primer sequences depict the mutated codons. The *phoN* ORF in the recombinant plasmids were sequenced completely using an automated DNA sequencer (ABI-PRISM 377) for the confirmation of targeted mutations. The mutant plasmids were subsequently transformed into the expression host individually for the overproduction of proteins. The proteins were expressed and purified to homogeneity as described earlier (*17*, *19*). The purified proteins were characterized by N-terminal amino acid sequencing and molecular mass determination by MALDI-TOF.

Enzymatic Assay and Kinetics. Protein concentration was determined by the modified Lowry's method using bovine serum albumin as the standard (*20*). The phosphatase activity of the purified proteins toward *p*NPP was assayed by monitoring the production of *p*-nitrophenylate (*p*NP) at 410 nm ($\Delta\epsilon = 17400\ M^{-1}\ cm^{-1}$). The standard reaction mixture (1.0 mL) for the assay of phosphatase activity was comprised of 100 mM sodium acetate buffer, pH 5.6, 5 mM *p*NPP, and a suitable quantity of enzyme and was incubated at 37 °C for 30 min. The reaction was stopped by the addition of 2 mL of 0.2 M NaOH, and absorbance of *p*NP was measured. The pH−activity profiles of the proteins were determined by using sodium acetate buffer for pH range 2.5−6.0 and Tris-HCl buffer for pH range 6.5−9.0 in the standard reaction mixture. Steady-state kinetic parameters for the hydrolysis of *p*NPP were determined by the analysis of initial reaction rates over a range of substrate concentrations ($0.1K_m$ to $10K_m$). The initial reaction rate (V_0) was plotted as a function of substrate concentrations using Microcal Origin, version 6.0, software. The values of V_{max} and K_m were derived from this plot using nonlinear curve fitting with the primary Michaelis−Menten equation. The turnover number (k_{cat}) was calculated from V_{max} using the equation $V_{max}/[E]$, where [E] is the enzyme concentration.

Crystallization and Data Collection. The recombinant purified PhoN protein crystallized in two forms with space groups *C*2 and $C222_1$, respectively (*19*). Briefly, the native PhoN crystals were grown by the vapor diffusion method using crystallization condition (12% PEG 6000 and 2% glycerol) in the presence of 25 mM sodium phosphate. Monoclinic crystals, which diffract to higher resolution data and were having four monomers in the asymmetric unit, were used for solving the three-dimensional structure. The native PhoN crystals were washed with stabilizing buffer (15% PEG 6000 and 2% glycerol) and were soaked in the same buffer containing 0.1 mM sodium tungstate for 1 h for preparing isomorphous crystals of the PhoN−tungstate complex. The crystals of the T159D mutant of PhoN (T159D-PhoN) isomorphous to the native crystals were harvested using the crystallization condition (15% PEG 6000, 25 mM potassium chloride, 5 mM magnesium sulfate) containing 25 mM sodium phosphate, pH 7.0. The diffraction intensity data for the native PhoN were recorded on R-AXIS IIC and those for the PhoN−tungstate and T159D-PhoN crystals on Mar345 imaging plate systems using Cu Kα radiation from a laboratory X-ray source. The intensity data were integrated using MOSFLM (*21*) and scaled, merged, and truncated using SCALA and TRUNCATE from CCP4 (*22*). Data collection statistics are summarized in Table 1.

Structure Solution and Refinement. A BLAST (*23*) search of the PDB (Protein Data Bank; *24*) revealed that the PhoN protein of *S. typhimurium* shares nearly 39% sequence identity with the Pho protein of *E. blattae* [PDB code 1D2T (*5*)]. The initial phases for the native PhoN were obtained by the molecular replacement method using the program AMoRe (*25*) with a model for the monomer of PhoN derived from the structure of the *E. blattae* Pho protein. A monomer as search model was employed in the molecular replacement search, as PhoN is known to exist as a dimer in contrast to the hexamer of the *E. blattae* Pho protein. The molecular replacement solution for each of the monomers expected in the asymmetric unit was carried out iteratively. Improvements of the molecular replacement phases were achieved by 4-fold noncrystallographic symmetry (NCS) averaging, coupled with solvent flattening and histogram matching using the DM program (*26*). The phases, refined with density modification and NCS averaging, were not combined with the calculated phases from the model obtained by molecular replacement, and thus the NCS refined phases are expected to be free from the model bias. The electron density maps computed with the improved phases were readily interpretable. A monomer of the PhoN molecule was fitted into the figure-of-merit weighted electron density maps computed using the density-modified, NCS refined phases. A dimer of biologically active PhoN was subsequently refined by a combination of simulated annealing/molecular dynamics and refinement of positional and individual thermal parameters using CNS (*27*), with intermittent model building using O (*28*). Strict NCS constraints for the second dimer in the asymmetric unit were used during the initial refinement of the structure using CNS. All four monomers were refined using NCS restraints during the final stages of structure refinement. The slow-cool simulated annealing refinement cycles used a heat stage at 3000 K with 25 K temperature decrement per cycle of dynamics. The manual corrections of the model were guided by σA corrected Fourier maps. The solvents from the electron density maps were identified only after the refinement of the models to a crystallographic *R*-value of ∼0.25. Refinement of the model performed using CNS with bulk solvent correction and maximum likelihood target was monitored by R_{work} and R_{free} (*29*). A phosphate anion (PO_4^{3-}) for each

Table 1: Crystallographic Data and Refinement Statistics

	native PhoN[a]	PhoN−tungstate[a]	T159D-PhoN[b]
data			
unit cell			
a (Å)	189.870	189.800	190.273
b (Å)	45.080	45.200	45.113
c (Å)	112.470	112.700	112.945
β (deg)	111.58	111.40	112.05
resolution limit (Å)	2.5	2.3	2.21
unique reflections	27475	37069	43054
completeness (%)	90.0	93.0	95.6
R_{merge} overall	0.087	0.060	0.079
in highest resolution shell[c]	0.243	0.110	0.182
mean *I*/mean σ(*I*) overall	8.1	9.7	12.7
in highest resolution shell[c]	2.3	3.2	4.7
Wilson *B* (Å^2)	34.0	30.3	28.9
model			
resolution range (Å)	20−2.5	20−2.3	20−2.21
final R_{work}	0.170	0.164	0.150
final R_{free} (5% of reflections)	0.214	0.211	0.207
no. of non-hydrogen atoms	7255	7328	7305
no. of protein atoms	6960	6982	7012
average thermal parameter (Å^2)	28.7	28.9	29.0
residues in core φ,ψ region of Ramachandaran plot (%)	94.8	94.7	94.8
SD[d] of χ_1 (pooled) (deg)	10.7	9.4	13.1
SD of χ_2 (t) (deg)	13.0	10.7	14.0
root-mean-square deviation			
bond distances (Å)	0.007	0.006	0.008
bond angles (°)	1.20	1.20	0.93
B, bonded main chain (Å^2)	1.25	1.28	2.03
B, bonded side chain (Å^2)	2.13	2.21	2.25

[a] The structure was refined using the CNS suite. [b] The structure was refined with the REFMAC suite. [c] The highest resolution shells for native PhoN, PhoN−tungstate, and T159D-PhoN are 2.50−2.64, 2.30−2.42, and 21−2.33 Å, respectively. [d] SD is the standard deviation.

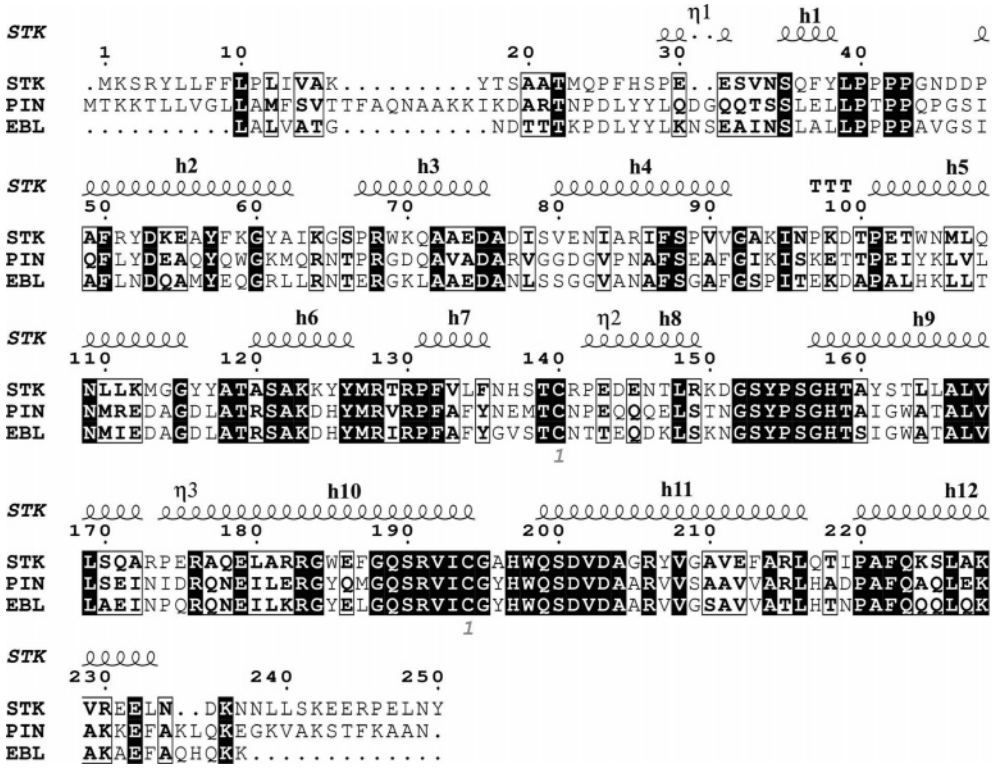

FIGURE 2: Sequence alignment of *S. typhimurium* PhoN (STK; Swiss-Prot accession number Q71EB8) with acid phosphatases of *P. intermedia* (PIN; Swiss-Prot accession number O87188) and *E. blattae* (EBL; Swiss-Prot accession number Q9S1A6). The residues are numbered as per the sequence of PhoN. The signal sequence is not shown for *E. blattae* acid phosphatase to match with residue numbering in the PDB entry 1D2T. Secondary structural elements for the PhoN protein, assigned using the DSSP suite (*35*), are shown above the sequence alignment. The conserved residues are boxed, and identical residues are shaded. The figure was prepared using ESPRINT (*36*).

monomer was additionally fitted into unaccounted spherical electron density and was refined for positional and thermal parameters. The spherical density was observed at more than 1.0σ level in the electron density maps computed with refined NCS phases, as well as with calculated phases from the partially refined models. The phosphorus atoms of phosphate anions refine to *B*-values of ~40 Å^2 with unit occupancy.

The refinement of the PhoN−tungstate structure was initiated using the atomic coordinates from the partially refined native PhoN with solvent molecules and phosphate ligands omitted. The positions of four tetrahedral tungstate anions (WO_4^{3-}) (one WO_4^{3-} for each monomer) were determined from the difference Fourier maps calculated with the PhoN−tungstate derivative and native PhoN amplitudes, and phases from the partially refined native PhoN structure. The four monomers of the PhoN−tungstate complex in the asymmetric unit were refined independently using CNS and O. The parameters for WO_4^{3-} used as restraints in the CNS refinement were obtained from the HICCUP server (*30*). The tungstate binding sites overlap with phosphates observed in the native structure. The tungsten atoms with 78 electrons refine to reasonable temperature factors of ~24 Å^2 with unit occupancy.

The refinement of the T159D-PhoN structure was initiated using the atomic coordinates of the refined PhoN structure after omitting the side-chain atoms of Thr-159, the solvent molecules, and the phosphate ligands from the coordinate list. The structure was refined using REFMAC5 (*31*) with bulk solvent correction and maximum likelihood target, and intermittent model editing using the O suite. Importantly, the $2F_o - F_c$ map showed clear density for the side-chain atoms of Arg-191 displaced from its position in native PhoN. Also, overlapping with the binding sites of phosphate and tungstate anions, an additional electron density was observed close to the active site Lys-123 and His-197 residues. A water molecule at this site refines to a reasonable *B*-value of nearly 20 Å^2 with unit occupancy.

Quality of the Structural Models. All three structural models have an *R*-factor below 17% against all of the observed data with $F/\sigma(F) \geq 0$ (Table 1). The evaluation using PROCHECK (*32*) and WHAT_CHECK software (*33*) revealed excellent stereochemistry of the structures, with nearly 95% of the residues in the core region of the Ramachandran plot with no disallowed (ϕ,ψ) combinations (Table 1). Electron density is well-defined everywhere except for the three N-terminal and nine C-terminal residues, and the atomic coordinates for these were not included in the refined models. Typically, the rms difference between corresponding C$^\alpha$ atoms of the two monomers of an active dimer of PhoN is 0.4 Å. Although the overall structures of PhoN−tungstate and T159D-PhoN are unchanged and match the native PhoN structure (the rms difference is 0.30 and 0.50 Å for the C$^\alpha$ atoms of the native PhoN dimer and those of PhoN−tungstate and T159D-PhoN, respectively), significant local changes do occur in the structure of T159D-PhoN.

RESULTS AND DISCUSSION

Overall Fold. The monomer fold is typical of an all-α protein and belongs to the "acid phosphatase/vanadium-dependent haloperoxidase" protein fold superfamily (SCOP; *34*), with nearly 73% of the amino acid residues comprising 12 helices (Figures 2 and 3A). The overall fold and secondary

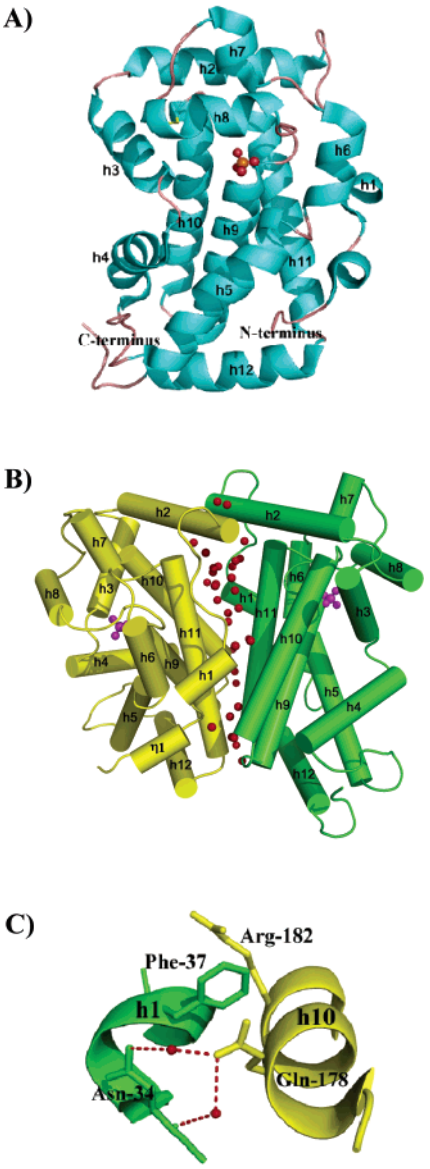

FIGURE 3: (A) Cartoon of the polypeptide chain trace of PhoN from residues 23 to 240. Phosphate atoms in the active site are shown as red balls. The helices are labeled as in Figure 2. (B) Cartoon of the PhoN dimer showing the two monomers (green and yellow) and water molecules (red spheres) observed at the dimer interface. Helices are shown as cylinders, and phosphate in the active site of each monomer is marked with magenta balls. The helices of each subunit are marked as in Figure 2. (C) Interaction of helix h1 of one monomer (green) with helix h10 of the other monomer (yellow). The figure was prepared with PyMol (*37*).

structure of PhoN monomer are essentially same as those of the Pho−molybdate complex of *E. blattae*: the rms difference is nearly 1.3 Å for the C^{α} atoms of PhoN and Pho−molybdate monomers.

Quaternary Structure. The PhoN crystals show phosphatase activity when soaked with a biochemical substrate like *p*NPP (*19*). In the crystallographic subunit, four copies of PhoN monomers form two independent dimers. The crystal structure is consistent with the homodimeric organization observed for the active protein in solution (*38*). The protein quaternary structure fileserver at the EBI (http://pqs.ebi.ac.uk/; *39*), based on the analysis of solvent-accessible surface area and gain in solvation energy, using the atomic coordinates of native PhoN, also predicts that the dimer of the PhoN protein observed in the crystal structure is physiologically relevant and is not due to crystallization effects. A loss of nearly 1850 $Å^2$ (∼14.5%) of solvent-accessible surface area and a gain of nearly −40 kcal/mol in solvation free energies of folding upon dimer formation are estimated. The two subunits of the dimer pack in back-to-back arrangement (Figure 3b). Direct hydrogen bonds between the residues of two subunits and bridged water molecules are involved at the dimer interface. Specifically, strong hydrogen bonds between the side-chain atoms of Arg-182, Arg-215, Tyr-207, and Tyr-185 with the main-chain atoms of Phe-37, Pro-174, Ala-181, and Tyr-207 are observed at the interface. But none of these residues are strictly conserved in PhoN orthologues (Figure 2). In addition, several hydrophobic residues are buried at the interface and may be contributing toward the stabilization of the PhoN dimer.

In comparison to the dimer of *S. typhimurium* PhoN, acid phosphatases of *E. blattae* and *Prevotella intermedia* are homohexamer (comprised of three dimers) and monomer, respectively (*5*, *40*). The varying oligomeric states of PhoN orthologues from different bacteria can be expected to have significance. Dramatic reduction in the phosphatase activity of the *P. intermedia* enzyme is observed when the residues of the conserved LPPPP motif are mutagenized (*40*). The reduction in the activity has been thought to be due to subtle conformational effects on the catalytic pocket probably caused by disturbance in the relative positions of helices h1 and h2. Both of these helices are stabilized at the dimer interface in the *S. typhimurium* PhoN structure. The aromatic side chain of Phe-37 of helix h1 resides in the groove of helix h10 of the other subunit and is sandwiched between Gln-178 and Arg-182 residues, and Asn-34 interacts with Gln-178 through bridging water molecules (Figure 3C). Also, helix h2 of one subunit is stabilized due to bridging water molecules with helix h2 of the other subunit in the *S. typhimurium* PhoN dimer. Stabilization of these helices can be expected to be responsible for marginal reduction in the activity of the L39T mutant of *S. typhimurium* PhoN (see Mutational Analysis below).

The Active Site. In the native PhoN structure a phosphate anion is observed in the active site of each monomer. A tungstate anion in the PhoN−tungstate structure replaces phosphate, whereas a solvent molecule occupies the oxyanion binding site in T159D-PhoN. The oxyanion binding site is surrounded by the invariant Lys-123, Arg-130, Ser-156, Gly-157, His-158, and Arg-191 residues, and His-197 is situated at the end of the cationic cavity nearly 12 Å from the molecular surface. The lone pair of $N^{\epsilon 2}$ of His-197 is directed toward the phosphorus atom of PO_4^{3-} ($N^{\epsilon 2}$−P ∼2.8 Å, angle $C^{\delta 2}$−$N^{\epsilon 2}$−P ∼140°) with the nitrogen atom oriented in-line with the phosphate oxygen O3 (angle $N^{\epsilon 2}$−P−O3 ∼170°). Although the orientation of PO_4^{3-} and WO_4^{3-} anions is the same, the tungstate anion binds deeper in the active site (Figure 4). The shorter distance between $N^{\epsilon 2}$ of His-197 and phosphorus atom, as compared to the distance between $N^{\epsilon 2}$ and tungsten (W) atom (Table 2), implies weaker interactions of the product inorganic phosphate. The two structures are consistent with our activity data: 1 mM tungstate inhibits the enzyme-catalyzed hydrolysis by ∼45%, whereas even 50 mM phosphate produces no inhibition.

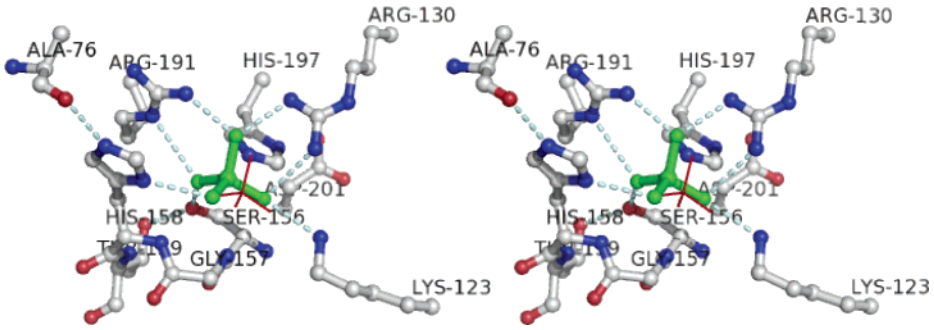

FIGURE 4: Stereoview showing interactions of tungstate anion (green) in the active site. Also shown is the phosphate anion (red lines) observed in the native PhoN structure. Hydrogen bonds/electrostatic interactions between the tungstate oxyanion and protein ligands are shown as dashed pale cyan lines. Carbon, nitrogen, and oxygen atoms of the protein are colored gray, blue, and red, respectively.

Table 2: Contacts of Ligands (Phosphate and Tungstate Anions) in the PhoN Active Site

phosphate anion			tungstate anion		
ligand (L) atom	protein (P) atom	L−P distance (Å)[a]	ligand (L) atom	protein (P) atom	L−P distance (Å)[a]
$P(PO_4^{3-})$	$N^{\epsilon 2}$(His-197)	2.8/2.9	$W(WO_4^{3-})$	$N^{\epsilon 2}$(His-197)	2.5/2.5
$O1(PO_4^{3-})$	O^{γ}(Ser-156)	3.0/3.1	$O1(WO_4^{3-})$	O^{γ}(Ser-156)	2.6/2.6
$O1(PO_4^{3-})$	N(His-158)	2.8/2.9	$O1(WO_4^{3-})$	N(His-158)	3.0/3.2
$O2(PO_4^{3-})$	$N^{\eta 1}$(Arg-130)	3.0/3.1	$O2(WO_4^{3-})$	$N^{\eta 1}$(Arg-130)	2.8/2.7
$O2(PO_4^{3-})$	$N^{\eta 2}$(Arg-130)	3.0/2.8	$O2(WO_4^{3-})$	$N^{\eta 2}$(Arg-130)	3.2/3.2
$O2(PO_4^{3-})$	$N^{\eta 2}$(Arg-191)	3.3/4.0	$O2(WO_4^{3-})$	$N^{\eta 2}$(Arg-191)	2.9/3.1
$O3(PO_4^{3-})$	$N^{\delta 1}$(His-158)	2.9/2.7	$O3(WO_4^{3-})$	$N^{\delta 1}$(His-158)	2.7/2.7
$O4(PO_4^{3-})$	N^{ζ}(Lys-123)	2.6/2.7	$O4(WO_4^{3-})$	N^{ζ}(Lys-123)	2.8/2.9
$O4(PO_4^{3-})$	N(Gly-157)	2.9/3.0	$O4(WO_4^{3-})$	N(Gly-157)	2.8/2.8
$O1(PO_4^{3-})$	N^{ϵ}(Arg-191)	3.8/4.0	$O1(WO_4^{3-})$	N^{ϵ}(Arg-191)	3.2/3.2

[a] Average values for A and C subunits and for B and D subunits, respectively. Subunits A and B constitute one active dimer, and subunits C and D form the second dimer in the crystallographic asymmetric unit. Contacts are defined as those with interatomic distances of 3.5 Å or less.

The active site of phosphate-bound PhoN resembles more closely the *E. blattae* Pho−molybdate complex (PDB code 1EOI) than the native Pho of *E. blattae*, where a sulfate anion is observed in the active site. In the Pho−sulfate structure the active site His-150 and Arg-183 residues (corresponding to His-158 and Arg-191 of the PhoN sequence; Figure 2) are displaced away from the phosphate binding site by more than 2 Å. In addition, the polypeptide segment 133−143 is highly flexible in the Pho−sulfate structure and gets ordered on binding of molybdate oxyanion in the active site (*5*). This segment (residues 141−151 of the PhoN sequence) adopts a stable helical structure (helix h8) in phosphate-bound PhoN, in the PhoN−tungstate complex, and in T159D-PhoN, even though the oxyanion is not observed in the active site of T159D-PhoN, and resembles closely the Pho−molybdate structure. The segment offers Leu-148 and Asp-151 in the active site. Leu-148 and Asp-151, being within a distance of 4 Å from phosphate binding site, could influence substrate binding and reaction kinetics.

The Leu-140 of the *E. blattae* Pho protein (corresponding to Leu-148 of PhoN) has been proposed by Ishikawa et al. (*5*) to act as a shield in protecting the phosphoenzyme intermediate from an attack by a water molecule. Leu-140 and Tyr-188 are situated above the molybdate binding site in acid phosphatase of *E. blattae*. Tyr-188 is substituted by Ala (Ala-196) in *S. typhimurium* PhoN. The hydrophobic side chain of Leu-148 in the phosphate-bound PhoN, PhoN−tungstate, and T159D-PhoN structures is displaced by more than 2.5 Å relative to its position in *E. blattae* Pho protein and is placed in such a way that it completely covers the oxyanion binding site. The structure of PhoN and conservation of the hydrophobic residue (Leu/Met) at position 148 in PhoN orthologues thus confirm the suggestion of Ishikawa et al.

The functional role of Asp-151, however, is not very clear. Asp-151 is substituted by asparagine or glutamine in PhoN orthologues. A side-chain oxygen atom of Asp-151 accepts hydrogen bonds from NH_3^+ groups of Lys-123 and Arg-130 in the PhoN structure. These hydrogen bonds are conserved also with asparagine (Asn-143) in the *E. blattae* Pho−molybdate complex. The residue at position 151, however, cannot be stabilizing the side-chain conformation of its hydrogen bond donor residues. In the *E. blattae* Pho−sulfate structure the side chains of Lys-115 and Arg-122 (corresponding to Lys-123 and Arg-130 of PhoN) are in the active conformation, while Asn-143 is placed at ~8 Å from these residues.

Interactions of Phosphate and the Phosphohistidyl Intermediate. The oxygen atoms of phosphate and tungstate groups are involved in electrostatic and hydrogen bond interactions to several protein side-chain and main-chain atoms (Table 2, Figure 4). The phosphate O2 atom, from the interatomic distances, can be expected to be fixed in its position due to electrostatic interactions with the side-chain NH_3^+ terminal groups of Arg-130 and Arg-191 and the phosphate O4 atom being stabilized by electrostatic interactions with the NH_3^+ group of Lys-123. The apical oxygen O3 of phosphate is within hydrogen bond distance from the $N^{\delta 1}$ atom of His-158. The interatomic distances are consistent with hydrogen bonds from the phosphate O1 atom to the side-chain O^{γ} of Ser-156 and the backbone nitrogen atom of His-158, and from the phosphate O4 atom to the backbone nitrogen atoms of Gly-157. In addition, the O1 oxygen of WO_4^{3-} accepts an additional hydrogen bond from the N^{ϵ}

atom of Arg-191, and this hydrogen bond is not observed for PO_4^{3-} in the phosphate-bound PhoN structure (Table 2). The two hydrogen bonds between the molybdate oxyanion and the side-chain nitrogen atoms of Arg-191 were also observed in the Pho−molybdate structure, and it was suggested that these interactions apparently stabilize the phosphoenzyme intermediate (*5*). On the basis of the crystal structure of the PhoN−tungstate complex, we believe the binding mode and interactions of the phosphoryl moiety of the phosphohistidine intermediate can be modeled. The three oxygen atoms of the phosphoryl group can be thought to occupy the same positions as three basal oxygen atoms (O1, O2, and O4) of the tungstate tetrahedron and are stabilized due to hydrogen bonds/electrostatic interactions with Lys-123, Arg-130, Ser-156, Gly-157, and Arg-191 residues. The displacement of the tungsten atom in the plane of basal oxygen atoms, to mimic phosphoryl bound in the active site, positions the tungsten atom at a distance of nearly 1.7 Å from $N^{\epsilon 2}$ of His-197, which is in agreement with the N−P distance observed in the phosphohistidine intermediates in the structures of phosphoglycerate mutase and nucleoside diphosphate kinase (*41*, *42*). The tungsten atom in the displaced position shall possess trigonal-bipyramidal geometry, like that observed for the molybdenum atom in the *E. blattae* Pho−molybdate structure. The molybdenum atom in the latter structure however is at a distance of nearly 2.0 Å from $N^{\epsilon 2}$ of His-197 (*5*).

His-158 and His-197 Exist in $N^{\epsilon 2}$-H and $N^{\delta 1}$-H Tautomeric Forms. The inward placement of the tungstate anion is accompanied with nearly 0.7 Å displacement of the side-chain imidazole of His-158. The movement of the His-158 side chain results in a hydrogen bond between $N^{\epsilon 2}$ of His-158 and the oxygen atom of Ala-76 (2.7 Å), which suggests that His-158 exists in $N^{\epsilon 2}$-H tautomeric form. Thus in view of the mechanistic details and for elucidation of the determinants, which can influence the pH optimum of the PhoN enzyme, $N^{\delta 1}$ of His-158 acts as a general acid/base during the catalysis.

The interatomic distance of 2.5 Å between $N^{\epsilon 2}$ of His-197 and W and the angle $C^{\delta 2}-N^{\epsilon 2}-W$ ~120° indicate that $N^{\epsilon 2}$ of His-197 is unprotonated and the lone pair of $N^{\epsilon 2}$ is directed toward the tungsten atom, suggesting that His-197 exists in the $N^{\delta 1}$-H tautomeric form. A distance of nearly 3.2 Å between $N^{\delta 1}$ of His-197 and the side-chain carboxylate of the invariant Asp-201, observed in the phosphate-bound PhoN and PhoN−tungstate complex, suggests that His-197 interacts with Asp-201 and that the latter can influence the tautomeric form or charge on the His-197 ring.

Mutational Analysis. The amino acid residues Thr-159, Asp-201, and distal Leu-39 were substituted with Asp, Asn, and Thr, respectively. The phosphatase activity of wild type as well as mutant proteins purified to homogeneity was determined at different pHs in the range 2.5−9.0 using *p*NPP as the substrate. The resulting pH−activity profile of the enzymes is shown in Figure 5, and the Michaelis−Menten parameters, k_{cat} and K_m, are given in Table 3.

The D201N mutant does not display any activity over the entire pH range of 2.5−9.0. The total loss of activity on substitution of the invariant Asp-201 with the Asn residue may be due to disturbance in the interaction between His-197 and Asp-201 (see section on Role of Asp-201).

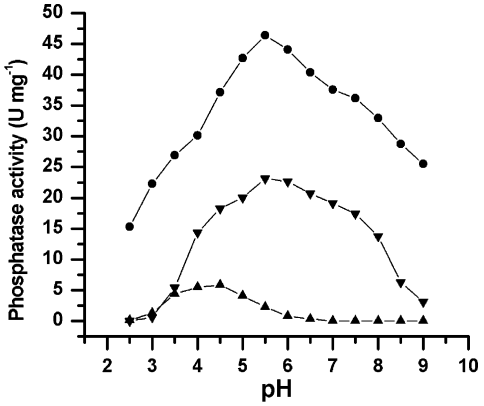

FIGURE 5: pH-dependent specific activity of the wild-type (●), L39T mutant (▼), and T159D mutant (▲) of the PhoN protein. The D201N mutant does not display phosphatase activity over the broad pH range of 2.5−9. One unit of phosphatase activity (U) is the micromoles of *p*NP released per minute in the standard reaction mixture. The values reported are the average of at least three independent experiments.

Table 3: Steady-State Kinetic Parameters for Phosphatase Activity Estimated at Different pH Values Using *p*NPP Substrate[a]

protein	pH of enzymatic assay	K_m (mM)	k_{cat} (s^{-1})	k_{cat}/K_m (s^{-1} mM^{-1})
wt-PhoN	5.5*	0.12	22.3	185.8
	4.0	0.10	14.5	145.0
T159D mutant	4.0*	0.25	3.7	14.8
	5.5	0.94	2.73	2.90
L39T mutant	5.5*	0.07	11.4	162.8
D201N mutant	2.5−9.0	ND[b]	ND[b]	ND[b]

[a] The values reported are the average of three independent experiments. The pH optimum of each protein is identified with an asterisk (*). [b] ND, the kinetic parameters could not be estimated due to nondetectable activity.

The T159D mutant displays catalytic efficiency reduced by nearly 12-fold as compared to that of native enzyme at acidic pH, and a total loss of activity for the T159D mutant is observed at basic pHs. The drastic reduction in the activity due to the substitution of Thr-159 with Asp, however, was unexpected. In the crystal structures of native PhoN as well as in the PhoN−tungstate complex, Thr-159 is a donor of a hydrogen bond to O^{γ} of Ser-156, and its substitution by aspartate could be expected to orient the hydrogen of the Ser-156 O^{γ} atom away from the phosphate oxygen. We had thus hypothesized that the T159D mutation could influence the hydrogen bond donor characteristics of the invariant Ser-156 to substrate phosphate and, as a result, expected that K_m might be affected without much influence on the turnover number, as direct involvement of Ser-156 and Thr-159 in catalysis has not been suggested previously. The pH−activity profile of the T159D mutant, however, can be rationalized on the basis of the 3D structure of the mutant protein and is in accordance with the pK_a of an aspartate residue.

In the T159D mutant structure solved using the crystals grown at pH 7.0, His-158 and His-197 residues are displaced from their active conformation, and Arg-191 is swung out of the active site and interacts with Asp-159 (see section on Role of Arg-191). The structure and the kinetic data suggest that the negatively charged Asp-159, at pH above its pK_a, is responsible for the displacement of Arg-191 away from the active site, which results in a total loss of activity. Under

acidic conditions (pH <5), the activity of the mutant is nearly 10% that of the native enzyme. At this acidic pH the side-chain carboxylate of aspartate can be expected to be neutral, and the guanidine of Arg-191 may be attracted toward it weakly.

The L39T mutant of *S. typhimurium* displays nearly 2-fold reduction in the enzymatic activity and marginal reduction (<10%) in the catalytic efficiency. Leu-39 in PhoN aligns to Leu-51 of *P. intermedia* acid phosphatase (Figure 2). In comparison, nearly 50 times reduction in k_{cat} and a factor of 3 increase in K_m in the L51T mutant of *P. intermedia* acid phosphatase have been reported (*40*). The L39T mutant of *S. typhimurium* PhoN, however, was very sensitive to SDS presence, as 0.001% SDS could reduce the phosphatase activity to 5% as compared to only about 10% loss in the activity of the wild-type enzyme (data not shown). It is possible that the hypersensitivity to SDS is linked to the oligomeric state of the protein, such that PhoN exists as a monomer in the presence of a small concentration of SDS, and the loss of activity of the L39T mutant of monomeric PhoN parallels the severe effect of L51T mutation in *P. intermedia* acid phosphatase.

In the absence of SDS, the PhoN protein is a dimer, and the observed ~50% reduction in the turnover number of the L39T mutant may be due to subtle conformational changes in the active site residues. Leu-39 is placed more than 12 Å away from the phosphate binding site in the PhoN structure. In silico modeling of the L39T substitution reveals that Thr at position 39 could interact with the side-chain hydroxyl of Tyr-154. In the PhoN structure the invariant Tyr-154 forms a strong hydrogen bond (2.6 Å) with the backbone oxygen of Pro-40, and its aromatic ring stacks against the Pro-42 ring. Structural superposition reveals that this hydrogen bond is conserved in the known structures of class A bNSAPs and vanadium-dependent haloperoxidases, despite poor sequence homology between these protein families (Figure 6). Most likely, the interaction of Tyr-154 stabilizes the loop harboring the active site scaffold forming residues ^{155}PSGH^{158}. The presence of the structurally conserved motif in the highly diverged family of proteins points to an important role of the hydrogen bond. We believe that the structural conservation and the striking similarity in the active site scaffold of these protein families may be linked with conformational stability and position of the invariant Tyr-154 due to its hydrogen bond with the polyproline motif. The substitutions in the LPPPP motif may influence the active site scaffold and thus the phosphatase activity through Tyr-154.

Role of the Invariant Arg-191. Both phosphate and tungstate anions interact with Lys-123, Arg-130, Ser-156, Gly-157, His-158, and Arg-191 residues in phosphate-bound PhoN and PhoN−tungstate complex structures. The active scaffold however is perturbed in the crystal structure of T159D-PhoN. Unexpectedly, the side chain of Arg-191, which stabilizes the substrate phosphate group as well the phosphoenzyme intermediate through hydrogen bond/electrostatic interactions, swings away from the phosphate binding site and toward the substituted Asp-159 in the T159D-PhoN structure (Figure 7). The $N^{\eta 2}$ of Arg-191, which interacts with phosphate oxygen in the native structure, is displaced by more than 6 Å from its position and is within hydrogen bond distance to the side-chain carboxylate oxygen

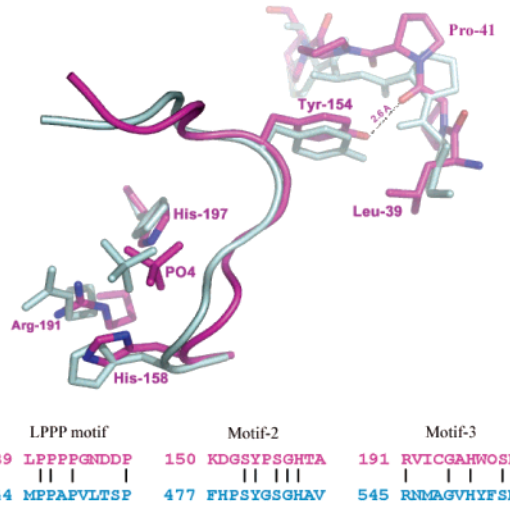

FIGURE 6: Structurally conserved motif in the highly diverged family of proteins. The loop harbors active site residues (^{154}YPSGH^{158}) and is stabilized by the interactions of highly conserved Tyr-154 with the distal ^{39}LPPPP^{43} motif (PhoN, magenta; vanadium-dependent bromoperoxidase, cyan, PDB code 1QHB). The inset shows the alignment of the conserved sequence motifs from these proteins. The coordinates of the *S. typhimurium* PhoN monomer and vanadium-dependent bromoperoxidase were superimposed using DaliLite (*43*; http://www.ebi.ac.uk/DaliLite/).

of the substituted Asp at position 159. The other carboxylate oxygen of Asp-159, as expected, accepts a hydrogen bond from the O^{γ} atom of Ser-156, which in the wild-type enzyme engages the substrate phosphate by donating a hydrogen bond. The reduced affinity of the substrate due to the loss of interactions with Arg-191 and Ser-156 residues in the T159D mutant is suggested by altered K_m that increases by a factor of nearly 7 at pH 5.5 (Table 3). Surprisingly, however, the most dramatic influence of the T159D mutation is observed on the imidazole side chains of activity-linked His-158 and His-197. The side chain of His-197, intriguingly, is oriented differently than that of the native structure due to nearly 170° rotation about the $C^{\beta}-C^{\gamma}$ bond and is displaced by about 0.8 Å from its position toward a solvent (Figure 7). The imidazole side chain of His-158 is also rotated about the $C^{\beta}-C^{\gamma}$ bond, and its $N^{\delta 1}$ atom is not pointing toward the phosphate binding site but interacts with a solvent. Both of the solvent molecules, which are hydrogen-bonded to the activity-linked His rings in T159D-PhoN, occupy the cavity created by the movement of Arg-191 and are not observed in the native PhoN structure.

In the altered conformational state, His-197 cannot carry out a nucleophilic attack on the electron-deficient phosphorus of the substrate phosphate group, nor is $N^{\delta 1}$ of His-158 in a position to act as an acid/base during the catalysis. The disturbance in active site thus results in the nearly total loss of phosphatase activity in the T159D mutant. Clearly, the active conformation of His-158 and His-197 residues is maintained due to steric constraints of the Arg-191 side-chain atoms. The role of the invariant Arg-191 in maintaining the active site scaffold is consistent with the nearly total loss of activity on substitution of Arg-191 with Ser in the *P. intermedia* PhoN orthologue (*9*). Further, the critical role of hydrogen bond donors at the position of the N^{ϵ} and $N^{\eta 1}$ atoms of Arg-191 is consistent with the nearly total loss of activity observed on substitution of equivalent arginine (Arg-217)

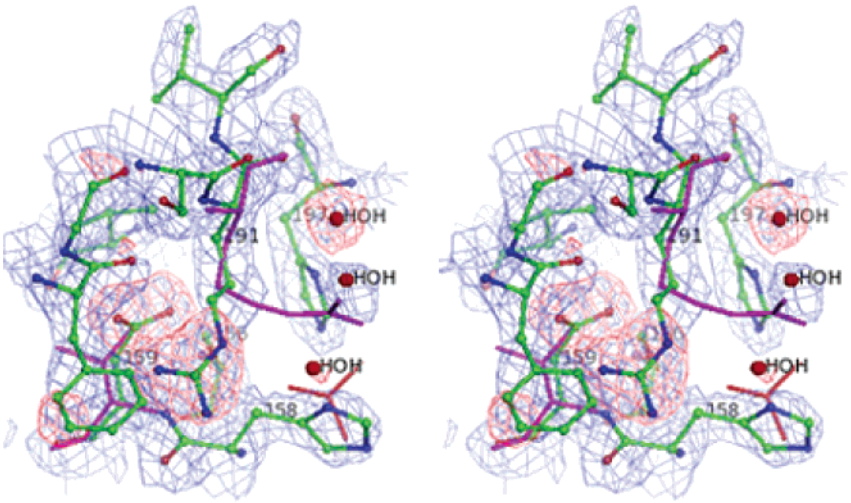

FIGURE 7: The first $2F_o - F_c$ (blue) and $F_o - F_c$ (pink) maps of the T159D mutant structure showing the displacement of the Arg-191 residue away from the active site and its influence on the conformation of the activity-linked His-158 and His-197 residues. The maps are drawn at 1.2σ and 3.2σ levels, respectively. The T159D mutant structure is shown in ball and stick representation with carbon, nitrogen, and oxygen atoms shown in green, blue, and red colors, respectively. Also shown are the side chains of the Arg-191 and Thr-159 residues (magenta) and phosphate (red) of the active native PhoN. The water molecules (HOH; red spheres), which occupy the void created by the displacement of Arg-191 in the T159D mutant, are marked. Both His-158 and His-197 are rotated by ~180° about the $C^{\alpha}-C^{\beta}$ bond resulting in the "flipping" of the side-chain imidazole groups, as compared to their conformation in the native protein.

with Lys in lipid phosphate phosphatase-1 of the PAP2 superfamily (*12*).

Search with SPASM (Server version 1.020303; http://portray.bmc.uu.se/cgi-bin/spasm/scripts/spasm.pl) for the active site scaffold, similar to that observed in PhoN, using the atomic coordinates of Lys-123, Arg-130, Ser-156, His-158, Arg-191, and His-197 residues of PhoN, revealed an excellent match of the atomic coordinates of these residues with those of vanadium-dependent haloperoxidases (PDB codes 1IDU, 1QHB, and 1QI9) with an rms difference of less than 0.75 Å. The apovanadium chloroperoxidase proteins have also been shown to possess reduced phosphatase activity (*7*). The substitution of Arg-490 (equivalent to Arg-191 of PhoN) with Ala in apovanadium chloroperoxidase leads to a total loss of phosphatase activity, while its R360A and K353A mutants (corresponding to Arg-130 and Lys-123 of PhoN) were observed to possess reduced phosphatase activity (*14*). Thus, in the vanadium-dependent chloroperoxidase family of proteins, Arg-490 can be expected to play a functional role as suggested here for *S. typhimurium* PhoN and not merely as a transition-state stabilizing residue as proposed earlier.

Role of the Invariant Asp-201. Asp-201 is conserved in class A bacterial nonspecific acid phosphatases and apyrase proteins. The other members of the PAP2 superfamily (except for glucose-6-phosphatases where glutamine aligns with the aspartyl residue) also harbor aspartate at this position. In the PhoN structure, Asp-201 is placed at nearly 7 Å from the substrate binding site and interacts with the nucleophile His-197: the $N^{\delta 1}$ atom of His-197 is within hydrogen bond distance (3.2 Å) to $O^{\delta 2}$ of Asp-201. The $O^{\delta 2}$ of Asp-201 also accepts a hydrogen bond from the main-chain amide group of Trp-198 and is within a distance of 2.6 Å from O^{γ} of Ser-153. $O^{\delta 1}$ of Asp-201 is an acceptor of a hydrogen bond from the $N^{\eta 1}$ atom of Arg-128 (2.8 Å). It has been shown from neutron diffraction studies that the hydroxyl of a carboxylate group cannot accept a hydrogen bond (*44*). Consequently, Asp-201 is expected to be negatively charged, as both of its carboxylate oxygen atoms are acceptors of hydrogen bonds in the PhoN structure. Further, the local environment around Asp-201 may be conserved in PhoN orthologues, as the spatial relationship among Arg-128, Ser-153, His-197, and Asp201 residues is virtually equivalent in three-dimensional structures of PhoN and *E. blattae* acid phosphatase, and these residues are conserved in class A bNSAPs.

The interaction between the $N^{\delta 1}$ atom of His-197 and the carboxylate of Asp-201 has been suggested to be important for enzyme function: for stabilizing the proton of $N^{\delta 1}$ by charge relay such that $N^{\epsilon 2}-P$ bond formation is facilitated (*4*) and for stabilization of the His-197 conformation (*5*). By analogy with the proteins having a catalytic His-Asp/Glu dyad, the functional role of Asp-201 can additionally be thought (i) to be stabilizing the $N^{\delta 1}$-H tautomer of His-197, thereby rendering the $N^{\epsilon 2}$ imidazole unprotonated, and (ii) to stabilize the positive charge on the His-197 ring that develops during the formation of the N−P bond. In the T159D-PhoN structure, the carboxylate group of Asp-201 superimposes onto that of native PhoN, but the imidazole side chain of His-197 is oriented differently by a nearly 170° rotation about the $C^{\beta}-C^{\gamma}$ bond and is displaced from its position toward a solvent. The reorientation of the His-197 side chain in the T159D mutant is not due to stabilization of the His-197 conformation, as the altered conformation with χ^1/χ^2 angles of −67°/−147° is less frequently observed [frequency of occurrence 13% (*45*)] as compared to the active conformation in native PhoN (χ^1/χ^2 −77°/−80°; frequency of occurrence ~29%). The closest approach of nearly 4.5 Å between His-197 ($C^{\delta 2}$ atom) and the carboxylate oxygens of Asp-201 suggests that His-197 does not interact with Asp-201 in the T159D mutant. The less frequently observed conformation of the His-197 side chain in the T159D mutant is stabilized by a hydrogen bond with a solvent molecule (2.9 Å) which fills the cavity created due to the displacement of Arg-191 away from the active site. The comparison of native PhoN and T159D-PhoN structures thus suggests that

the position of the His-197 nucleophile in the active form of the enzyme is not fixed due to His-Asp interactions but owing to spatial constraints imposed due to the side-chain atoms of Arg-191.

The mutagenic and structural data further suggest that the functional role of Asp-201 may not be limited only to the stabilizing $N^{\delta1}$-H tautomer of His-197. Asp-201 is situated at the N-terminal of helix h11, and the side chain of Asp-201 adopts the most frequently observed conformation (75% occurrence) with χ^1/χ^2 values of nearly $-54°/-40°$. The same χ^1/χ^2 combination most frequently occurs (66%) for the asparagine side chain (*45*). A simple modeling exercise reveals that the side-chain amide oxygen of Asn-201 in the most frequently observed conformation should be within hydrogen bond distance to $N^{\delta1}$ of His-197. Thus, the D201N mutant could be expected to possess some activity if Asp-201 stabilizes the $N^{\delta1}$-H tautomer of His-197. The substitution of Asp-201 however results in a total loss of phosphatase activity over a broad pH range of 2.5−9.0.

The D201N mutagenic data do not identify further if Asp-201 participates in charge relay or if its negative charge stabilizes the positive charge on the His-197 ring, as substituted asparagine cannot carry out either of the functions. The analysis of the available structures, however, provides insight into the functional role of Asp-201. Strong and conserved hydrogen bonds from O^{γ} of Ser-153 and the main-chain amide of Trp-198 can be expected to partially satisfy the valence of the Asp-201 $O^{\delta2}$ atom, which suggests that complete transfer of the proton from His-197, as required for the charge-relay mechanism, is not very likely. Further, a distance of nearly 3.7 Å between $N^{\delta1}$ of His-197 and the carboxylate oxygen of Asp-201 is observed in the structure of the *E. blattae* Pho−molybdate complex (*5*). Molybdate being a transition-state mimic, this long distance does not support the charge-relay mechanism for class A bacterial nonspecific acid phosphatases, as proton shuttling between the charge couple will be essential for the charge relay. Typically, a strong hydrogen bond with a donor−acceptor distance of less than 3 Å may be expected to facilitate charge relay, as observed for the active site imidazole−carboxylate couple of the carbonic anhydrase I enzyme (*46*). By comparison, as electrostatic force varies inversely as the square of the distance, a negatively charged Asp-201 even at a distance of 3.7 Å could stabilize the positive charge on the His-197 ring. The mutagenic and kinetic data and crystal structures thus suggest that negatively charged Asp-201 might play a major role in catalysis by stabilizing the positive charge on His-197 that develops during the formation of the phosphoenzyme intermediate. Similar functional roles for aspartate/glutamate of the His-carboxylate catalytic dyad in phosphatidylinositol-specific phospholipase C, and for human tyrosyl-DNA phosphotransferase, have been proven recently (*47*, *48*).

Alternatively, if, owing to the local environment, asparagine adopts a conformation (χ^1/χ^2 of $-46°/24°$) with the terminal amide nitrogen toward His-197, the imidazole side chain of the latter may get displaced or flipped away from the active position due to steric conflicts between the protonated $N^{\delta1}$ of His-197 and the protons on $N^{\delta2}$ of asparagine. Such a possibility cannot be ruled out completely. The displacement of active histidine (His-57) that forms a catalytic dyad with Asp-102 was observed to be mainly responsible for the loss of activity in the D102N mutant of trypsin due to steric conflicts (*49*).

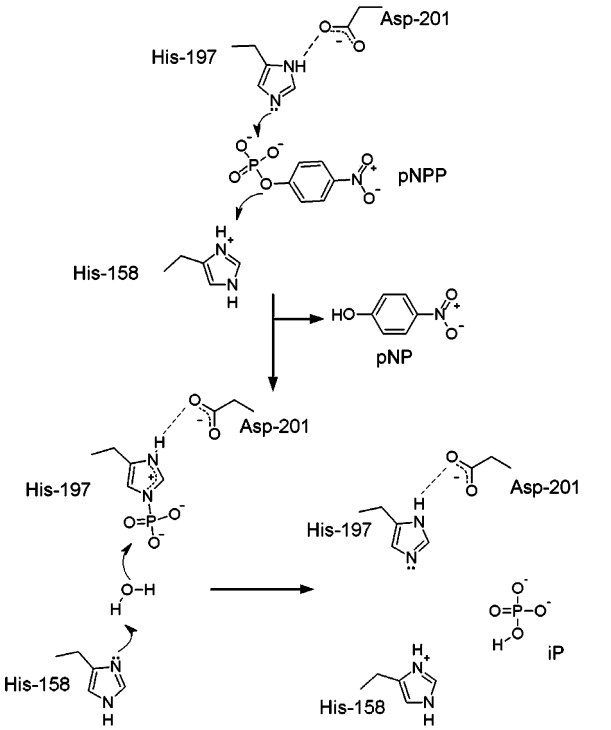

FIGURE 8: Reaction mechanism. The figure was prepared using ACD/ChemSketch version 10.

Mechanistic Aspects. The phosphatase reaction is generally believed to proceed in two steps. The first step involves transfer of the phosphoryl moiety from the monoester substrate to His-197 due to hydrolysis of the P−O bond resulting in formation of the phosphoenzyme intermediate and release of alcohol. In the second step a nucleophile activated by His-158 attacks the phosphorus center of the phosphoenzyme intermediate, leading to the release of either inorganic phosphate (if an hydroxyl moiety is the nucleophile) or a phosphorylated organic compound (if the nucleophile is a free hydroxyl group of an organic molecule).

Model of the First Half-Reaction. The geometry of the PhoN active site dictates an S_N2-type mechanism in which $N^{\epsilon2}$ of His-197 carries a nucleophilic attack on the P center of the substrate phosphate moiety. The phosphorus thus transiently is in a trigonal-bipyramidal state. A proton transfer from $N^{\delta1}$ of His-158 facilitates the release of the alcohol moiety from the enzyme active site. The phosphoryl is stabilized in the active site due to hydrogen bonds/electrostatic interactions, as observed for the three basal oxygen atoms (O1, O2, and O4) of tungstate in the PhoN−tungstate structure. The $N^{\epsilon2}$−P bond formation can be facilitated by Asp-201 due to stabilization of the positive charge that develops on the His-197 ring (Figure 8). The total loss of phosphatase activity in the D201N mutant is consistent with the suggested functional role of Asp-201. The His^{197}-Asp^{201} couple may also facilitate the key requirement that His-197 exist as an $N^{\delta1}$-H tautomer.

Model of the Second Half-Reaction. The N−P bond in phosphohistidine is highly unstable (*50*). The release of product orthophosphate is expected to be facilitated by the attack of activated water on the P center (*5*). In agreement with the mechanistic proposals for other phosphatases, the

attacking water must be a good nucleophile and in-line with the P−N bond for S_N2 reaction. Modeling for a water in such a position reveals that the water should be in proximity to the O3 position of the phosphate observed in the native PhoN structure. Further, a proton acceptor, acting as a base, should be within hydrogen-bonding distance from the water molecule at this position. As proposed earlier (*5*), the only protein atom in proximity to this site is $N^{\delta1}$ of His-158. His-158 from the structure of the PhoN−tungstate complex is expected to be in an $N^{\epsilon2}$-H tautomeric form. Proton abstraction from a water molecule thus should localize the positive charge on the $N^{\delta1}$ of His-158, which will also explain the microscopic reversibility that $N^{\delta1}$ is the donor of a proton during the first step of the next catalytic cycle. Our recent results are in agreement with the proposal, as the pH optimum of the PhoN enzyme could be shifted by influencing electrostatic and solvent accessibility of His-158 (*17*).

In conclusion, using a combination of mutagenic, kinetic, and structural data, we show for the first time that the invariant Arg-191 plays a crucial role in maintaining the active conformation of activity-linked histidyl residues in bacterial nonspecific acid phosphatases. We show from the crystal structure of the T159D mutant of PhoN that Arg-191 sterically restricts the side-chain imidazole groups of His-158 and His-197 residues. Contrary to the earlier suggestion, we find that the invariant Asp-201 may be functioning as a negative charge to stabilize the positively charged His-197 ring that develops on formation of the phosphoenzyme intermediate. The total loss of enzymatic activity in the D201N mutant over a broad pH range and the conserved local environment of Asp-201 in a number of structures are consistent with this functional role of Asp-201. We also show that the varying oligomeric states of PhoN orthologues in different bacteria may have significance. The mutation in the conserved ^{39}LPPPP^{43} motif of *S. typhimurium* PhoN has much less influence on the phosphatase activity as compared to that observed for *P. intermedia* acid phosphatase: PhoN is a dimer and the orthologous protein of *P. intermedia* exists as a monomer. Also, in the present work a structurally conserved region harboring the active site forming the ^{155}PSGH^{158} motif is thought to be stabilized by interactions between Tyr-154 and the distal polyproline motif. Our analysis also suggests that amino acid residues of vanadium-dependent haloperoxidases, those that align with Arg-191 and Tyr-154 of PhoN, may also play a crucial role in maintaining the active site scaffold of the former family of proteins.

ACKNOWLEDGMENT

We are deeply indebted to Prof. T. P. Singh, All India Institute of Medical Sciences, Delhi, for helping in the acquisition of diffraction intensity data, the National Facility for Photolabelling and Peptide Sequencing in Biomolecular Systems, Indian Institute of Technology, Mumbai, for the N-terminal sequencing of the proteins, and Dr. R. Mukhopadhyaya for helping in DNA sequencing.

REFERENCES

1. Rossolini, G. M., Schippa, S., Riccio, M. L., Berlutti, F., Macaskie, L. E., and Thaller, M. C. (1998) Bacterial nonspecific acid phosphohydrolases: physiology, evolution and use as tools in microbial biotechnology, *Cell. Mol. Life Sci. 54*, 833−850.
2. Thaller, M. C., Schippa, S., and Rossolini, G. M. (1998) Conserved sequence motifs among bacterial, eukaryotic, and archaeal phosphatases that define a new phosphohydrolase superfamily, *Protein Sci. 7*, 1647−1652.
3. Bateman, A., Coin, L., Durbin, R., Finn, R. D., Hollich, V., Griffiths-Jones, S., Khanna, A., Marshall, M., Moxon, S., Sonnhammer, E. L., Studholme, D. J., Yeats, C., and Eddy, S. R. (2004) The Pfam protein families database, *Nucleic Acids Res. 32*, D138−D141.
4. Neuwald, A. F. (1997) An unexpected structural relationship between integral membrane phosphatases and soluble haloperoxidases, *Protein Sci. 6*, 1764−1767.
5. Ishikawa, K., Mihara, Y., Gondoh, K., Suzuki, E., and Asano, Y. (2000) X-ray structures of a novel acid phosphatase from *Escherichia blattae* and its complex with the transition-state analog molybdate, *EMBO J. 19*, 2412−2423.
6. Sigal, Y. J., McDermott, M. I., and Morris, A. J. (2005) Integral membrane lipid phosphatases/phosphotransferases: common structure and diverse functions, *Biochem. J. 387*, 281−293.
7. Hemrika, W., Renirie, R., Dekker, H. L., Barnett, P., and Wever, R. (1997) From phosphatases to vanadium peroxidases: a similar architecture of the active site, *Proc. Natl. Acad. Sci. U.S.A. 94*, 2145−2149.
8. Stuky, J., and Carman, G. M. (1997) Identification of a novel phosphatase sequences motif, *Protein Sci. 6*, 469−472.
9. Chen, X., Ansai, T., Barik, S., and Takehara, T. (2003) Kinetic and site-directed mutagenesis studies of *Prevotella intermedia* acid phosphatase, *Protein Pept. Lett. 10*, 53−59.
10. Sarli, S., Nicoletti, M., Schippa, S., Del Chierico, F., Santapaola, D., Valenti, P., and Berlutti, F. (2005) Ala160 and His116 residues are involved in activity and specificity of apyrase, an ATP-hydrolysing enzyme produced by enteroinvasive *Escherichia coli*, *Microbiology 151*, 2853−2860.
11. Ghosh, A., Shieh, J. J., Pan, C. J., Sun, M. S., and Chou, J. Y. (2002) The catalytic center of glucose-6-phosphatase. HIS176 is the nucleophile forming the phosphohistidine-enzyme intermediate during catalysis, *J. Biol. Chem. 277*, 32837−32842.
12. Zhang, Q. X., Pilquil, C. S., Dewald, J., Berthiaume, L. G., and Brindley, D. N. (2000) Identification of structurally important domains of lipid phosphate phosphatase-1: implications for its sites of action, *Biochem. J. 345*, 181−184.
13. Toke, D. A., McClintick, M. L., and Carman, G. M. (1999) Mutagenesis of the phosphatase sequence motif in diacylglycerol pyrophosphate phosphatase from *Saccharomyces cerevisiae*, *Biochemistry 38*, 14606−14613.
14. Renirie, R., Hemrika, W., and Wever, R. (2000) Peroxidase and phosphatase activity of active-site mutants of vanadium chloroperoxidase from the fungus *Curvularia inaequalis*. Implications for the catalytic mechanisms, *J. Biol. Chem. 275*, 11650−11657.
15. Macaskie, L. E., Bonthrone, K. M., and Rouch, D. A. (1994) Phosphatase-mediated heavy metal accumulation by a *Citrobacter* sp. and related enterobacteria, *FEMS Microbiol. Lett. 121*, 141−146.
16. Basnakova, G., Stephens, E. R., Thaller, M. C., Rossolini, G. M., and Macaskie, L. E. (1998) The use of *Escherichia coli* bearing a phoN gene for the removal of uranium and nickel from aqueous flows, *Appl. Microbiol. Biotechnol. 50*, 266−272.
17. Makde, R. D., Dikshit, K., and Kumar, V. (2006) Protein engineering of class-A non-specific acid phosphatase (PhoN) of *Salmonella typhimurium*: modulation of the pH-activity profile, *Biomol. Eng. 23*, 247−251.
18. Sambrook, J., and Russell, D. W. (2001) *Molecular Cloning: A Laboratory Manual*, 3rd ed., Cold Spring Harbor Laboratory Press, New York.
19. Makde, R. D., Kumar, V., Rao, A. S., Yadava, V. S., and Mahajan, S. K. (2003) Purification, crystallization and preliminary X-ray diffraction studies of recombinant class-A non-specific acid phosphatase of *Salmonella typhimurium*, *Acta Crystallogr. D59*, 515−518.
20. Miller, G. L. (1959) Protein determination for large numbers of samples, *Anal. Chem. 31*, 964.
21. Powell, H. R. (1999) The Rossmann Fourier autoindexing algorithm in MOSFLM, *Acta Crystallogr. D55*, 1690−1695.
22. CCP4 (1994) The CCP4 suite: programs for protein crystallography, *Acta Crystallogr. D50*, 760−763.
23. Altschul, S. F., Madden, T. L., Schaffer, A. A., Zhang, J., Zhang, Z., Miller, W., and Lipman, D. J. (1997) Gapped BLAST and PSI-BLAST: a new generation of protein database search programs, *Nucleic Acids Res. 25*, 3389−3402.

24. Berman, H. M., Westbrook, J., Feng, Z., Gilliland, G., Bhat, T. N., Weissig, H., Shindyalov, I. N., and Bourne, P. E. (2000) The Protein Data Bank, *Nucleic Acids Res. 28*, 235−242.
25. Navaza, J. (1994) AMoRe: an automated package for molecular replacement, *Acta Crystallogr. A50*, 157−163.
26. Cowtan, K. D. (1994) DM program, in *Joint CCP4 ESF-EACBM Newsletter 31*, pp 34−38.
27. Brunger, A. T., Adams, P. D., Clore, G. M., DeLano, W. L., Gros, P., Grosse-Kunstleve, R. W., Jiang, J. S., Kuszewski, J., Nilges, M., Pannu, N. S., Read, R. J., Rice, L. M., Simonson, T., and Warren, G. L. (1998) Crystallography & NMR system: A new software suite for macromolecular structure determination, *Acta Crystallogr. D54*, 905−921.
28. Jones, T. A., Zou, J. Y., Cowan, S. W., and Kjeldgaard, M. (1991) Improved methods for building protein models in electron density maps and the location of errors in these models, *Acta Crystallogr. A47*, 110−119.
29. Brunger, A. T. (1997) Free R value: Cross validation in crystallography, *Methods Enzymol. 277*, 366−396.
30. Kleywegt, G. J., and Jones, T. A. (1998) Databases in protein crystallography, *Acta Crystallogr. D54*, 1119−1131.
31. Vagin, A. A., Steiner, R. A., Lebedev, A. A., Potterton, L., McNicholas, S., Long, F., and Murshudov, G. N. (2004) REFMAC5 dictionary: organization of prior chemical knowledge and guidelines for its use, *Acta Crystallogr. D60*, 2184−2195.
32. Laskowski, R., MacArthur, M. W., Moss, D. S., and Thornton, J. M. (1993) PROCHECK: a program to check the stereochemical quality of protein structures, *J. Appl. Crystallogr. 26*, 283−291.
33. Hooft, R. W., Vriend, G., Sander, C., and Abola, E. E. (1996) Errors in protein structures, *Nature 381*, 272.
34. Murzin, A. G., Brenner, S. E., Hubbard, T., and Chothia, C. (1995) SCOP: a structural classification of proteins database for the investigation of sequences and structures, *J. Mol. Biol. 247*, 536−540.
35. Kabsch, W., and Sander, C. (1983) Dictionary of protein secondary structure: pattern recognition of hydrogen-bonded and geometrical features, *Biopolymers 22*, 2577−2637.
36. Gouet, P., Robert, X., and Courcelle, E. (2003) ESPript/ENDscript: Extracting and rendering sequence and 3D information from atomic structures of proteins, *Nucleic Acids Res. 31*, 3320−3323.
37. Delano, W. L. (2002) *The PyMOL molecular graphics system*, DeLano Scientific, San Carlos, CA.
38. Weppelman, R., Kier, L. D., and Ames, B. N. (1977) Properties of two phosphatases and a cyclic phosphodiesterase of *Salmonella typhimurium*, *J. Bacteriol. 130*, 411−419.
39. Henrick, K., and Thornton, J. M. (1998) PQS: a protein quaternary structure file server, *Trends Biochem. Sci. 23*, 358−361.
40. Ansai, T., Chen, X., Barik, S., and Takehara, T. (2002) Conserved proline residues near the N-terminus are important for enzymatic activity of class A bacterial acid phosphatases, *Arch. Biochem. Biophys. 408*, 144−146.
41. Bond, C. S., White, M. F., and Hunter, W. N. (2001) High resolution structure of the phosphohistidine-activated form of *Escherichia coli* cofactor-dependent phosphoglycerate mutase, *J. Biol. Chem. 276*, 3247−3253.
42. Morera, S., Chiadmi, M., LeBras, G., Lascu, I., and Janin, J. (1995) Mechanism of phosphate transfer by nucleoside diphosphate kinase: X-ray structures of the phosphohistidine intermediate of the enzymes from *Drosophila* and *Dictyostelium*, *Biochemistry 34*, 11062−11070.
43. Holm, L., and Park, J. (2000) DaliLite workbench for protein structure comparison, *Bioinformatics 16*, 566−567.
44. Ramanadham, M., Jakkal, V. S., and Chidambaram, R. (1993) Carboxyl group hydrogen bonding in X-ray protein structures analysed using neutron studies on amino acids, *FEBS Lett. 323*, 203−206.
45. Lovell, S. C., Word, J. M., Richardson, J. S., and Richardson, D. C. (2000) The penultimate rotamer library, *Proteins 40*, 389−408.
46. Kumar, V., and Kannan, K. K. (1994) Enzyme-substrate interactions. Structure of human carbonic anhydrase I complexed with bicarbonate, *J. Mol. Biol. 241*, 226−232.
47. Zhao, L., Liao, H., and Tsai, M. D. (2004) The catalytic role of aspartate in a short strong hydrogen bond of the Asp274-His32 catalytic dyad in phosphatidylinositol-specific phospholipase C can be substituted by a chloride ion, *J. Biol. Chem. 279*, 31995−32000.
48. Davies, D. R., Interthal, H., Champoux, J. J., and Hol, W. G. (2002) Insights into substrate binding and catalytic mechanism of human tyrosyl-DNA phosphodiesterase (Tdp1) from vanadate and tungstate-inhibited structures, *J. Mol. Biol. 324*, 917−932.
49. Sprang, S., Standing, T., Fletterick, R. J., Stroud, R. M., Finer-Moore, J., Xuong, N. H., Hamlin, R., Rutter, W. J., and Craik, C. S. (1987) The three-dimensional structure of Asn102 mutant of trypsin: role of Asp102 in serine protease catalysis, *Science 237*, 905−909.
50. Kim, Y., Pesis, K. H., and Matthews, H. R. (1995) Removal of phosphate from phosphohistidine in proteins, *Biochim. Biophys. Acta 1268*, 221−228.

BI062180G